Inter-reflection Compensation of Immersive Projection Display by Spatio-Temporal Screen Reflectance Modulation

Shoichi Takeda, Daisuke Iwai, and Kosuke Sato, *Member, IEEE*

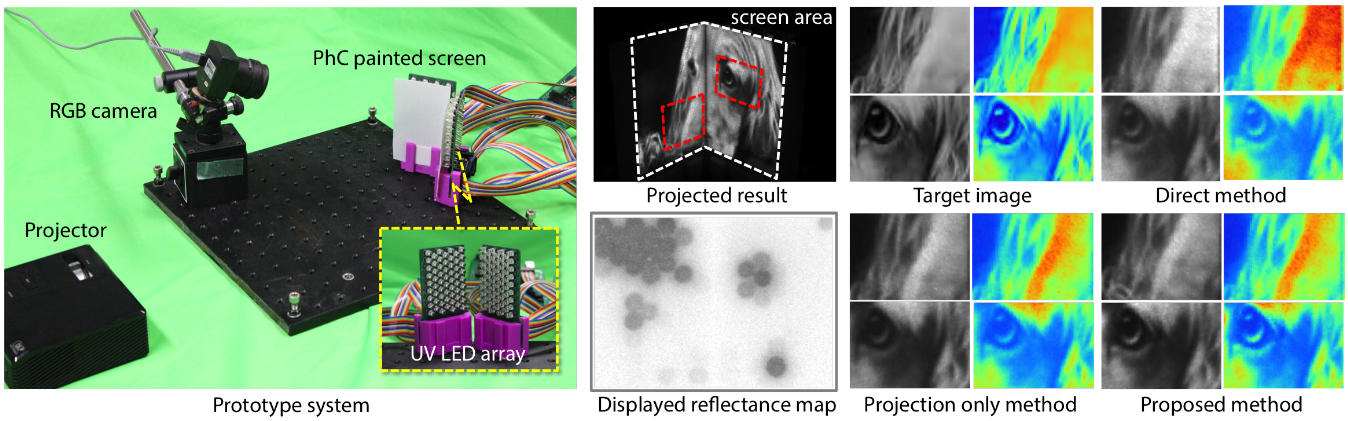

Fig. 1. Proposed technique compensates for the inter-reflections of a projected image onto a concave immersive projection screen: (**left**) prototype system comprising a projector, an RGB camera, a screen painted with a photochromic compound, and UV LED arrays that control the reflectance pattern of the screen; (**middle-top**) projected result of the dog image (Section 4.2) obtained using the proposed method; (**middle-bottom**) reflectance pattern displayed on the screen (rectified using homography); (**right**) close-ups of projected results and the pseudo-color visualizations of their intensity values. There are two areas in the direct method's result where undesirable intensity elevation is found, i.e., around the nose of the dog and around the left eye. While the projection only (conventional) method [22] can compensate for the elevated intensity in the nose area, the proposed method can compensate for the elevated intensity in both areas.

Abstract—We propose a novel inter-reflection compensation technique for immersive projection displays wherein we spatially modulate the reflectance pattern on the screen to improve the compensation performance of conventional methods. As the luminance of light reflected on a projection surface is mathematically represented as the multiplication of the illuminance of incident light and the surface reflectance, we can reduce undesirable intensity elevation because of inter-reflections by decreasing surface reflectance. Based on this principle, we improve conventional inter-reflection compensation techniques by applying reflectance pattern modulation. We realize spatial reflectance modulation of a projection screen by painting it with a photochromic compound, which changes its color (i.e., the reflectance of the screen) when ultraviolet (UV) light is applied and by controlling UV irradiation with a UV LED array placed behind the screen. The main contribution of this paper is a computational model to optimize a reflectance pattern for the accurate reproduction of a target appearance by decreasing the intensity elevation caused by inter-reflection while maintaining the maximum intensity of the target appearance. Through simulation and physical experiments, we demonstrate the feasibility of the proposed model and confirm its advantage over conventional methods.

Index Terms—Reverse radiosity, inter-reflection compensation, immersive projection display.

1 Introduction

Immersive projection displays, which use screens of various concave shapes such as L-shaped corners, cubes, cylinders, and hemispherical domes, are widely used in cinemas and virtual reality (VR) systems. These displays suffer from inter-reflections of projected light, which unfavorably elevate the lowest intensity of a projected result; consequently, they lead to significant contrast deterioration. As a result, the degradation of image quality disturbs user immersion. Researchers have investigated the inter-reflection issue and have proposed various inter-reflection compensation techniques that digitally modify input images prior to projection such that the degradation of the projected image quality is reduced [3, 22]. Simply speaking, for L-shaped corner or cube screens, these techniques decrease pixel intensities at the corners of the projection screens. However, the compensation performance of these methods is limited due to the additive nature of inter-reflection and the absence of negative projected light.

Research focused on decreasing the lowest intensity of projection light has been primarily conducted in the context of high dynamic range (HDR) projection. In the last decade, various researchers have successfully decreased black offsets, which, because a projector cannot project pure black, are unavoidable intensities, by using two spatial light modulators (SLM) to block light [11, 17, 26]. However, these HDR projection techniques do not solve the inter-reflection issue in principle. For example, consider an attempt to display a completely black image on the left side of an L-shaped corner screen and a uniform white image on the right side using an HDR projector that can project completely dark images. In this case, some portion of the light

- *Shoichi Takeda is with Osaka University. E-mail: shoichi.takeda@sens.sys.es.osaka-u.ac.jp.*
- *Daisuke Iwai is with Osaka University. E-mail: daisuke.iwai@sys.es.osaka-u.ac.jp.*
- *Kosuke Sato is with Osaka University. E-mail: sato@sys.es.osaka-u.ac.jp.*

Manuscript received 18 Sept. 2014; accepted 10 Jan. 2015. Date of Publication 20 Jan. 2015; date of current version 23 Mar. 2015. For information on obtaining reprints of this article, please send e-mail to: reprints@ieee.org.

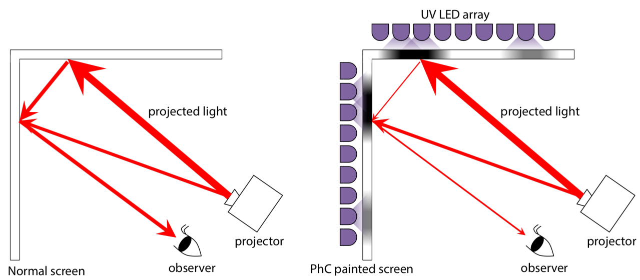

Fig. 2. Concept of the proposed method: (left) inter-reflection occurs on concave projection screen with a normal uniformly white surface; (right) the proposed reflectance pattern modulation decreases the intensity elevation due to inter-reflection.

reflected from the right side of the screen inevitably reflects to the left side and increases the black offset. Therefore, a completely dark image is no longer displayed on the left side of the screen.

We realize HDR projection by applying a different approach, i.e., we spatially modulate the reflectance pattern of the projection surface to reduce the black offsets [4, 14, 28]. The luminance of light reflected on a projection surface is mathematically represented as the multiplication of the illuminance of incident light and the surface reflectance; thus, the projected result can be made darker by decreasing the surface reflectance. This approach, in contrast to other HDR projection approaches, has the potential to solve the inter-reflection issue. In the example mentioned above, by setting the reflectance of the left screen to zero, we can make the reflected light from the right screen not reflect on the left screen; consequently, a completely dark image is displayed on the left screen.

In this paper, we propose an inter-reflection compensation technique in which we spatially modulate the reflectance pattern on a screen to improve the performance of previous inter-reflection compensation methods (Fig. 2). Iwai et al. [14] realized a spatial reflectance modulation of a projection screen by painting it with a photochromic compound (PhC) that changes color (i.e., the reflectance of the screen) when ultraviolet (UV) light is applied, and by controlling UV irradiation using a UV LED array behind the screen. We propose to apply this technology to inter-reflection compensation. The main contribution of this work is a computational model to optimize a reflectance pattern for accurate reproduction of a target appearance by decreasing the intensity elevation caused by inter-reflection while maintaining the maximum intensity of the target appearance. We evaluate the feasibility of the proposed model and confirm its advantage over conventional methods through a simulation experiment. We also conduct a physical experiment to demonstrate the inter-reflection compensation performance using currently available PhCs.

To summarize, we provide the following contributions:

- We propose an inter-reflection compensation technique that combines spatial surface reflectance modulation with a conventional projection image modification technique.
- We develop a computational model to optimize the reflectance pattern of a projection screen painted with a PhC that is controlled by UV LED arrays.
- We conduct a simulation experiment to validate the proposed principle.
- We demonstrate the inter-reflection compensation performance using currently available PhCs through a physical experiment.

2 Related Works

Four research fields—photometric and radiometric compensation, inter-reflection compensation, HDR projection, and projection surface reflectance modulation—are closely related to the proposed method. Here, we describe the related fields; and discuss the development of the proposed method.

2.1 Photometric and Radiometric Compensation

Photometric and radiometric compensation is a well-studied research topic to display desired colors on various types of surfaces including non-planar and textured ones. Even for a simple (i.e., planar and uniformly white) screen, projection images should be pre-corrected to compensate for the vignetting effect (i.e., peripheral area of projected image becomes darker than the central) [19]. For more general surfaces, a camera is applied to measure the reflectance properties in a per-pixel basis, which are then used to compute projection colors to correctly display desired colors [5]. Recent techniques significantly improve projected results in terms of color reproduction accuracy [8] and spatial resolution [21]. However, most of the previous techniques do not consider global illumination effects except for occlusions and defocus blurs [12, 13, 23], and thus, do not work correctly when projected pixels are inter-reflected.

2.2 Inter-reflection Compensation

Previous inter-reflection compensation techniques fall broadly into two categories: reverse radiosity and reverse light transport approaches. The reverse radiosity approach divides a concave screen surface into small patches, and reversely solves the radiosity equation iteratively [3] or analytically [22, 27]. In computer graphics, the radiosity technique is applied to compute the amount of light energy transferred among patches. The reverse light transport approach uses a camera to measure surface appearance when each projected pixel is turned on. The measurement is stored as a light transport matrix (LTM) with which we can estimate a displayed appearance including any global illumination effects when an input image is projected. In addition, we can compute an input image to display a desired projected result using the inverse LTM [32]. Generally, an LTM is a very large matrix (e.g., 1 million by 1 million pixels); consequently, computation of its inversion incurs an enormously high computational cost. Thus, researchers have proposed more efficient methods, such as utilizing the sparse characteristics of LTM [32], separating the direct and indirect (global) components of reflections [9], applying a stratified approach [24], and a simulation-based solution [18].

The reverse radiosity approach was developed for projection screens with simple shapes (e.g., cubic, cylindrical, and hemispherical), while the inverse light transport approach was developed for more complex shapes. In addition, the inverse light transport approach requires a huge amount of time for LTM measurement, which must be performed whenever a single component of a system (e.g., the pose/position of a camera/projector or the shape/reflectance of a screen) is changed. Because screen shapes of immersive projection displays are normally simple and we modulate screen reflectance patterns for different target images, we have developed our method based on a reverse radiosity method [22, 27].

2.3 HDR Projection

The contrast or dynamic range of a projection system is defined as the ratio of maximum to minimum intensity. In principle, projectors form images by attenuating the maximum intensity from light sources; therefore, a common strategy to realize HDR projectors is to reduce the minimum intensity (i.e., black offset). However, current SLMs cannot block light from a light source perfectly; thus, it is difficult for commercially available projectors to display images containing completely black portions where the black offset is zero. Following pioneering work by Seetzen et al. [26], HDR projectors with very low black offsets have been realized by applying the double modulation principle—the intensity of the light from a light source is attenuated twice at different SLMs. Seetzen et al. proposed projecting images onto a transmissive LCD, which is regarded as the second modulator [26], and Kusakabe et al. proposed using two liquid crystal on silicon (LCoS) micro-displays in a projector [17]. Recently, an analogue

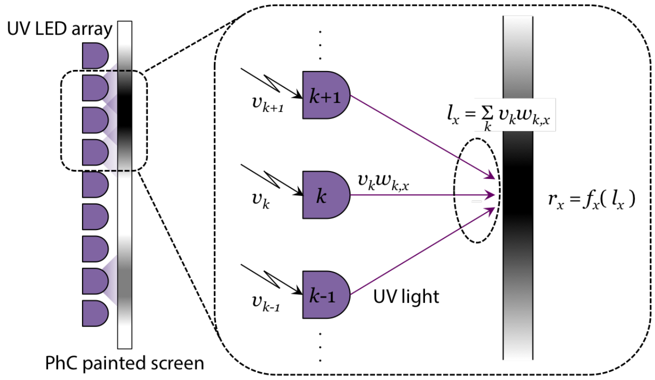

Fig. 3. Reflectance pattern modulation model of PhC and UV LED.

micromirror array (AMA) was used as the first modulator to reallocate the light energy from a light source to realize a low level of black offset and higher peak luminance [11].

As mentioned in Section 1, these HDR projection techniques cannot solve the inter-reflection issue. In this study, we apply the double modulation principle. We regard the spatial modulation of surface reflectance as the second modulation to reduce artifacts caused by the inter-reflections of projected light.

2.4 Projection Surface Reflectance Modulation

Surface reflectance modulation for projection display has primarily been investigated in the context of HDR or high contrast displays [4]. Essentially, this technique uses a flat printed paper (e.g., a photograph) as a screen and projects the same image content onto it. When the contrast of the projector is c_1:1 and that of the screen is c_2:1, the contrast of the system is theoretically increased to c_1c_2:1. This principle is then applied to boost the contrast of various objects, such as optical microscopy specimens [6] and replicas of historically important objects printed using a full-color three-dimensional (3D) printer [28]. Note that reflectance modulation is only applicable for static images because physically printed reflectance patterns are generally static. Recently, we have addressed this limitation by applying a PhC whose color can be controlled dynamically by adjusting the amount of UV irradiation [14].

To the best of our knowledge, projection surface reflectance modulation has not been applied to inter-reflection compensation for immersive projection displays. Because dynamic and interactive visual information is crucial for VR systems, an inter-reflection compensation technique for displaying dynamic image content on immersive projection displays is necessary. Therefore, we apply a spatio-temporal screen reflectance modulation technique using the PhC based approach [14] to inter-reflection compensation.

3 Inter-reflection Compensation using Reflectance Pattern Modulation

We summarize two fundamental techniques, i.e., reflectance pattern modulation using PhC and inter-reflection compensation based on reverse radiosity, in Sections 3.1 and 3.2, respectively. We describe the proposed approach—an inter-reflection compensation method combining projection image correction with reflectance pattern modulation—in Section 3.3.

For simplicity, we only consider one color channel. Note that this simplification does not entail a loss of generality. We also assume that projection screens are diffuse surfaces and that projected images are focused.

3.1 Reflectance Pattern Modulation

As shown in Fig. 3, we spatially modulate the reflectance pattern of a PhC-painted projection screen using an UV LED array. A target reflectance pattern is reproduced based on [14] as follows.

The reflectance of a PhC monotonically decreases as the illuminance of the radiated UV light increases. The relation between the reflectance of a PhC-painted screen at a surface patch x and the incident illuminance of UV light at that patch is expressed as:

$$r_x = f_x(l_x), \tag{1}$$

where r_x, l_x, and f_x denote reflectance, incident illuminance, and a monotonically decreasing function, respectively.

Because UV light is spread from each LED, each patch on the screen is radiated from multiple LEDs simultaneously. A normalized input value sent to the k-th LED is denoted v_k $(0 \leq v_k \leq 1)$ (Fig. 3). The illuminance of UV light radiated from the k-th LED with input value 1.0 (i.e., $v_k = 1.0$) at patch x is denoted as $w_{k,x}$. Assuming that the relation between an input value sent to an LED and the resulting UV output is linear, the illuminance at x from the k-th LED with v_k can be computed as $v_k w_{k,x}$. Consequently, the UV illuminance at x radiated from n LEDs can be computed as the sum of the illuminance from the LEDs as:

$$l_x = \sum_k v_k w_{k,x}. \tag{2}$$

Suppose a target reflectance at x is represented as $\tilde{r}_x$, the actual input value $\hat{v}_k$ for each LED in the array must be determined by minimizing the sum of squared errors of the generated reflectance from the target reflectance:

$$\hat{V} = \arg\min_V \sum_x \|\tilde{r}_x - f_x(l_x)\|_2, \tag{3}$$
$$\text{subject to } \; 0 \leq {}^\forall v_k \leq 1,$$

where V represents the set of input values $v_k \in V$. The least squares method is applied to find the input values.

3.2 Reverse Radiosity

We formulate our inter-reflection compensation method based-on the reverse radiosity approach. Radiosity is a global illumination algorithm that solves the rendering equation for scenes with diffuse surfaces [7]. Suppose that an immersive projection surface is divided into N small patches (i.e., $x = 1, 2, \ldots, N$). For each pair of patches x and x', a form factor $F_{xx'}$, which describes how well the patches can see each other, is computed as follows:

$$F_{xx'} = \frac{1}{A_x} \int_{A_{x'}} \int_{A_x} \frac{\cos\phi_{dA_x} \cos\phi_{dA_{x'}}}{\pi r^2_{dA_x dA_{x'}}} H_{dA_x dA_{x'}} \, dA_x dA_{x'}, \tag{4}$$

where $A_x, A_{x'}$ are the areas of patches x, x' respectively. $\phi_{dA_x}, \phi_{dA_{x'}}$ are the angles between the line from x to x' and the normal vectors of x and x' respectively. $r_{dA_x dA_{x'}}$ is the distance between the patches. $H_{dA_x dA_{x'}}$ is a visibility function, which is always 1 for normal immersive projection screens. B_x is the radiosity (reflection of both direct and indirect illumination) of patch x, and E_x is the emitted light (reflection of direct illumination from projectors). Thus, the radiosity equation can be expressed as

$$B_x = E_x + r_x \sum_{x'=1}^{N} F_{xx'} B_{x'}. \tag{5}$$

The radiosity equations of N surfaces are then represented as the following matrix equations:

$$E = KB, \tag{6}$$

$$K = \begin{bmatrix} 1 - r_1 F_{11} & -r_1 F_{12} & \cdots & -r_1 F_{1N} \\ -r_2 F_{21} & 1 - r_2 F_{22} & \cdots & -r_2 F_{2N} \\ \vdots & \vdots & \ddots & \vdots \\ -r_N F_{N1} & -r_N F_{N2} & \cdots & 1 - r_N F_{NN} \end{bmatrix}, \tag{7}$$

$$B = \begin{bmatrix} B_1 \\ \vdots \\ B_N \end{bmatrix}, E = \begin{bmatrix} E_1 \\ \vdots \\ E_N \end{bmatrix}. \tag{8}$$

Equation 6 represents the analytical solution of reverse radiosity [22, 27], from which we can compute the set of emitted light E from a target radiosity map $\tilde{B} = [\tilde{B}_1\ \tilde{B}_2\ \ldots\ \tilde{B}_N]^t$. As mentioned above, E_x is the reflection of direct illumination from the projector; thus, we can compute projection color p_x (input color value to a projector) from E_x by the following equation:

$$p_x = g_x(\frac{E_x}{r_x}), \tag{9}$$

where g_x is a per-patch function representing the relation between a projection color and the illuminance of a projected pixel on a projection surface at x. Because projection color should be within a certain range (e.g., $0 \leq p_x \leq 255$ for an ordinary 8-bit projector), g_x also clips the value outside the range. g_x can be calibrated in advance using a well-known technique for radiometric compensation of projector-camera systems [5]. In summary, we can compute an inter-reflection compensating projection image $P \ni p_x$ to accurately reproduce a target radiosity map $\tilde{B}$ on a surface with the reflectance pattern $R \ni r_x$.

3.3 Simultaneous Optimization of Projection Image and Reflectance Pattern

Our goal is to optimize the projection image and the reflectance pattern to compensate inter-reflection. The optimization problem is formulated as

$$\hat{P}, \hat{R} = \underset{P,R}{\arg\min} \|\tilde{B} - K^{-1}E\|_2. \tag{10}$$

We need to simultaneously optimize the projection image and reflectance pattern. However, the reverse radiosity technique described in Section 3.2 only optimizes a projection image for a given reflectance pattern.

To solve Eq. 10, we apply an iterative method. Suppose the reflectance pattern computed at the i-th iteration is $R^{(i)}$, then the inter-reflection compensating projection image $P^{(i)}$ for this reflectance pattern is computed using Eqs. 6 and 9. Next, we estimate a radiosity map $B^{(i)}$, which is displayed when the image $P^{(i)}$ is projected on the surface with reflectance pattern $R^{(i)}$ through inverse computation of Eqs. 6 and 9 as follows:

$$E_x^{(i)} = g_x^{-1}(p_x^{(i)})r_x^{(i)}, \tag{11}$$

$$B^{(i)} = {K^{(i)}}^{-1}E^{(i)}. \tag{12}$$

We apply the Bi-CGSTAB method [30] to compute the inverse of $K^{(i)}$, which is generally a huge matrix. Then, we compute the error between the target and estimated radiosities as follows:

$$e_x^{(i)} = B_x^{(i)} - \tilde{B}_x. \tag{13}$$

Because a patch x is illuminated with the illuminance of $B_x^{(i)}/r_x^{(i)}$, the reflectance component of the error is extracted as:

$$\frac{e_x^{(i)}}{B_x^{(i)}/r_x^{(i)}} = \frac{r_x^{(i)}}{B_x^{(i)}} e_x^{(i)}. \tag{14}$$

We update the reflectance value as:

$$\bar{r}_x^{(i+1)} = r_x^{(i)} - \phi \frac{r_x^{(i)}}{B_x^{(i)}} e_x^{(i)}, \tag{15}$$

where ϕ is a constant weight. In practice, $r_x^{(i)}/B_x^{(i)}$ is almost constant over a projection surface because low (high) reflectance normally leads to low (high) radiosity. Therefore, we can also use the following simpler method to update the reflectance value.

$$\bar{r}_x^{(i+1)} = r_x^{(i)} - \phi e_x^{(i)}. \tag{16}$$

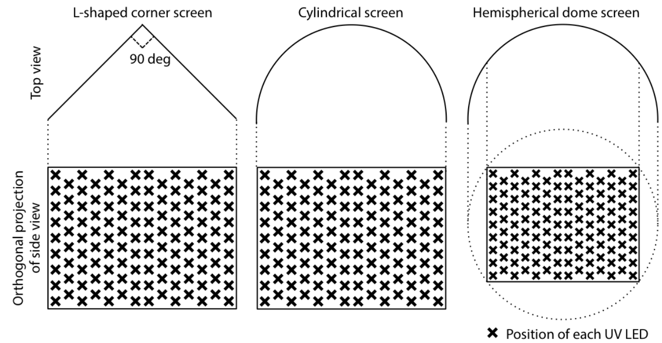

Fig. 4. Screens and UV-LED placements in the simulation experiment.

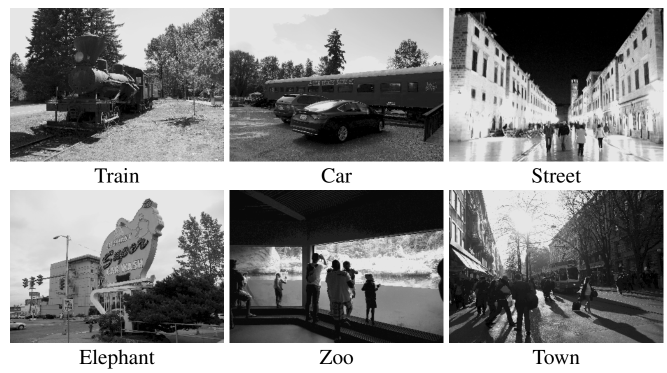

Fig. 5. Simulation experiment target images.

Note that the updated reflectance pattern $\bar{R}^{(i+1)} \ni \bar{r}_x^{(i+1)}$ normally has higher frequency components than the displayable reflectance pattern modulated by the PhC and UV LEDs. Therefore, we compute displayable pattern using the method described in Section 3.1. Specifically, we compute the optimum LED values $\hat{V}$ to display $\bar{R}^{(i+1)}$ using Eq. 3 and compute the displayable reflectance pattern $R^{(i+1)} \ni r_x^{(i+1)}$ using Eqs. 1 and 2.

The iteration is terminated when the number of iteration i exceeds a predefined number M or the difference of the mean squared error (MSE) of $e_x^{(i)}$ from the previous iteration becomes less than a predefined threshold ε. Then, the optimized projection image $\hat{P}$ and reflectance pattern $\hat{R}$ are obtained as $P^{(i)}$ and $R^{(i)}$ at the termination, respectively.

4 Experiment

We conducted simulation and physical experiments to validate the proposed method. First, we performed simulations under various experimental conditions to evaluate the characteristics of the proposed method (Section 4.1). Then, we conducted a physical experiment using a prototype system to validate the feasibility of the proposed method (Section 4.2).

4.1 Simulation

As shown in Fig. 4, for the simulation experiment, we prepared three semi-immersive projection screens (L-shaped corner, cylindrical, and hemispherical dome). Six different natural images were used as target appearances (or target radiosity maps), as shown in Fig. 5. The purpose of each simulation is that the orthogonal projection of projected result from the side view of each screen correctly reproduces a target appearance. The reflectance pattern of each screen was modulated by an array of UV LEDs which is set up in a honeycomb structure as shown in Fig. 4. The UV light from the LEDs was distributed all over the screen. The point spread function (PSF) of each LED is an

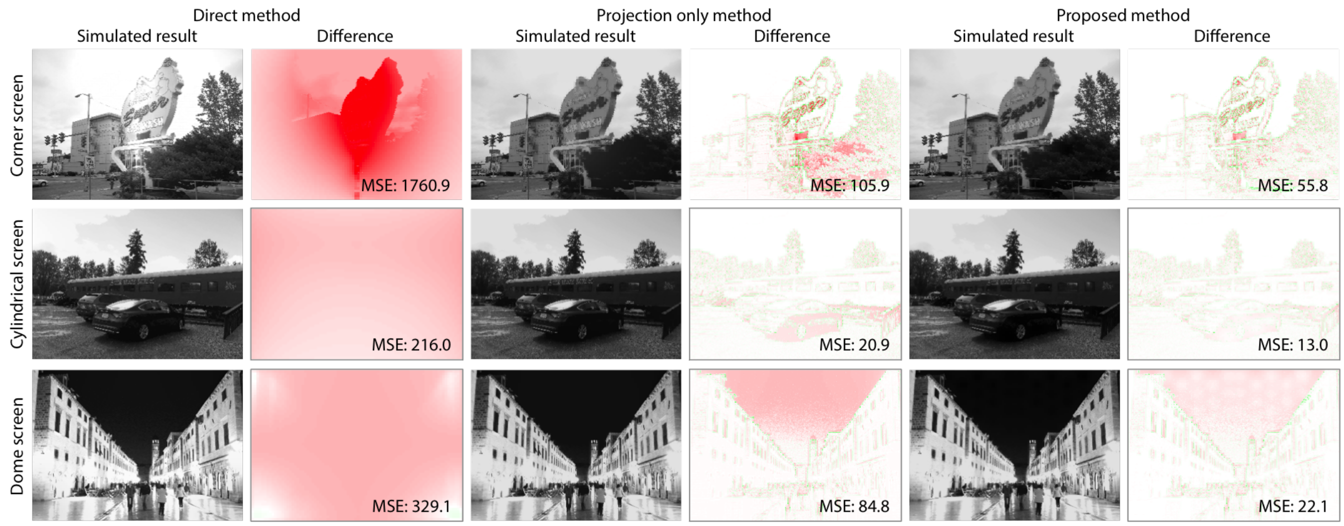

Fig. 6. Simulated results. Note that in the difference visualizations, red (green) colors indicate that the simulated results have higher (lower) intensity than the target appearances.

Table 1. Averaged MSEs in the simulation experiment.

	direct	projection only	proposed
corner	1272.6	105.9	**53.2**
cylindrical	209.6	21.0	**13.4**
dome	270.5	38.8	**18.8**

isotropic two-dimensional (2D) Gaussian distribution. The number of patches in each screen is 84×60 for all screen shapes.

We compared three different methods, i.e., **direct**, **projector only**, and the **proposed** method. In the direct method, a target image is projected onto a screen directly, i.e., neither inter-reflection compensation nor reflectance pattern modulation are applied. In the projector only method, only inter-reflection compensation is applied. A previously proposed reverse radiosity method [22] was used to modify a projection image, which was then projected onto a screen. The proposed method applies the proposed technique, i.e., both the projection image and the reflectance pattern are optimized to compensate inter-reflections. In this simulation experiment, we set the threshold for termination of the iteration process $\varepsilon = 1.0$ and updated the reflectance pattern using Eq. 15. There are nine conditions in the simulation experiment (i.e., 3 screens × 3 methods). Note that we only provide some of the simulation results in the paper; please refer to the supplementary material for other results.

Figure 6 shows sets of a target image, a simulated result, a difference visualization between the target and the result, and the MSE. The results show that the proposed method displays the most similar images among the three methods for all combinations of target images and screens. In particular, the direct method provides unnaturally bright images around the central part of each screen due to the inter-reflection of projected light. The projection only method can decrease a certain amount of unnatural intensity elevation. Compared to these conventional methods, such artifacts are much less apparent in the results obtained with the proposed method. In addition to the qualitative observations, we compare the averaged MSEs (Table 1). Thus, we confirm that the images displayed using the proposed method are most similar to the target images under all screen conditions. The proposed method is the most effective particularly under the corner screen condition, where the proposed method displayed images with MSEs of 1/24 and 1/2 times lower on average than the direct and projection only methods respectively.

Here, we evaluate our iterative method for simultaneous optimization of a projection image and a reflectance pattern. Figure 7 shows

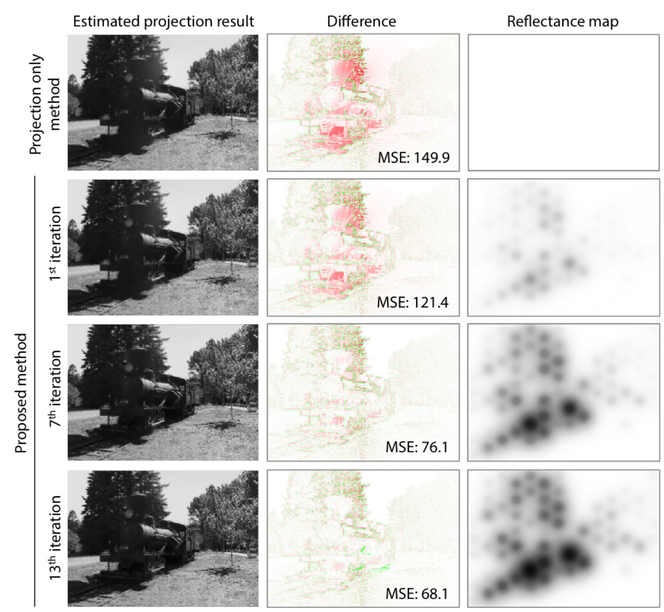

Fig. 7. Projection results, difference visualizations with MSE values, and reflectance maps for some iteration processes.

an estimated projection result, a difference image with its MSE value, and a reflectance pattern at each iteration process. These were simulated using the proposed method with the corner screen and the target train image. Figure 8 summarizes the MSE values of all combinations of screens and target images for all iteration processes. The results confirm that the reflectance pattern is updated through the iteration processes. In addition, our iteration method reduce the MSE, which reaches a plateau after a certain number of iterations. The processing time for each iteration ranged from 0.6 to 1.1 seconds.

4.2 Physical Experiment

We built a prototype system and conducted an experiment. As shown in Fig. 1(left), the system comprises a PhC-painted L-shaped corner screen, two 2D UV-LED arrays, an RGB camera (Point Grey Research Chameleon camera, 1280×960 pixels), and a projector (Acer K10, 100 ANSI lumen). We mixed three types of PhCs such that the mixed material appears gray when exposed to UV light. The combination of

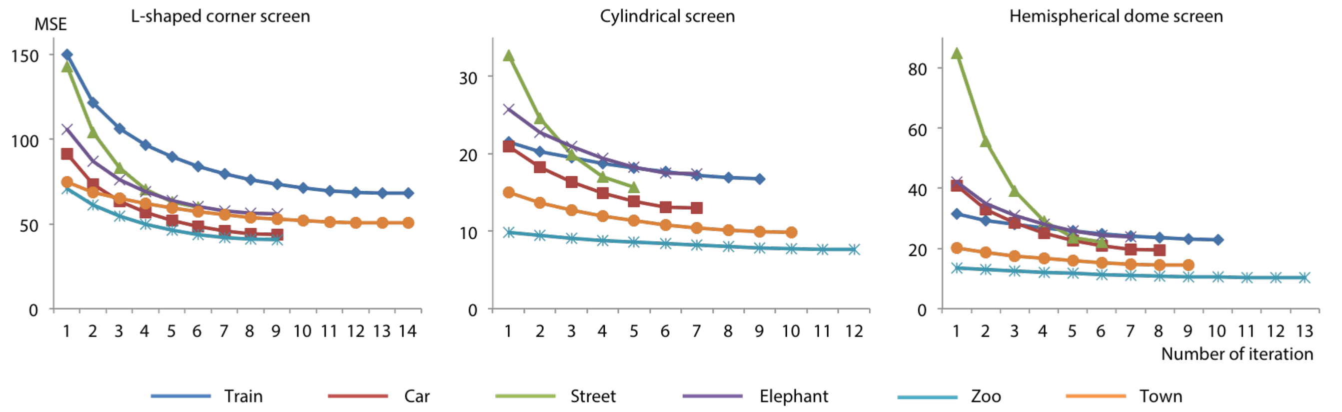

Fig. 8. MSE for each iteration process in the simulation experiment.

PhCs was PSP-54 (20 %), PSP-33 (22.5 %), and PSP-73 (57.5 %), which are produced by Yamada Chemical Co., Ltd. These materials, which are originally solid powders, are mixed with liquid polymethyl methacrylate (PMMA), so that we can paint the resulting liquid solution on the screen. Each LED array comprises 60 UV LEDs (Nitride Semiconductors Co., Ltd. NS365L-5RLQ) in a honeycomb structure that modulate UV intensities on the screen based on pulse width modulation (PWM) using an Arduino Uno and LED drivers. We painted the combined material on a 140×100 mm^2 sheet of white fabric (Amundsen, 100% polyester) folded 90 degrees at the center to form an L-shaped corner screen. The parameters of f_x and $w_{k,x}$ were calibrated for the reflectance pattern modulation. The camera-based calibration process is described in the literature [14]. It took around 1 minute to modulate the surface reflectance from the highest to the lowest values with the maximum UV intensity. We set the threshold for termination of the iteration process $\varepsilon = 1.0$ and updated the reflectance pattern using Eq. 16.

Similar to the simulation experiment described in Section 4.1, we compared the results among the three methods (i.e., direct, projection only, and proposed methods). Four different images (**complex**, **meal**, **room**, and **dog**) were used as target appearances for each method. Thus, there were twelve sets of experimental results (i.e., 3 methods $\times$ 4 targets). Figure 9 shows the results of three targets (complex, meal, and room)—each target image, the projected results of the three different methods, and their pseudo-color visualizations. Figure 10 shows the displayed reflectance patterns. In addition, Fig. 1 shows the results of the remaining target appearance (i.e., dog). Note that the results were captured using the RGB camera and then rectified using a simple homography transformation.

By comparing the pseudo-color visualizations between the target images and the direct method's results, it is confirmed that the direct method significantly elevates the black level around the corner of the screen due to inter-reflection. In addition, the projected results become darker in some parts that were originally bright in the target appearances. This occurs because the pixels were projected at an oblique angle to the surface. This loss of intensity does not orrur in the other methods because they take this effect into account in the reverse radiosity process, especially in the computation of E_x. Comparing the pseudo-color visualizations between the target images and the projection only method's results, we found that the reproducibility of dark parts is improved over the direct method. However, we also found that some bright parts, such as the hair accessory in the complex image and the right part of a circular dish in the meal image, are darker than the target images. These artifacts are caused by the projector's inter-reflection compensation, which can sometimes overly decrease the intensities of some parts of a projection image to reduce inter-reflections due to the projector's limited dynamic range. On the other hand, the proposed method visually reproduces both dark and bright parts better than the compared methods.

Table 2. SSIM values of projected results in physical experiment.

	Direct	Projection only	Proposed
Complex image	0.506	0.503	**0.517**
Meal image	0.497	0.496	**0.509**
Room image	0.638	0.639	**0.651**
Dog image	0.609	0.644	**0.661**

We evaluated the image qualities of the simulated results using the structural similarity index (SSIM), which is a method for assessing the perceptual quality of a distorted image compared to the original [31]. The SSIM values are shown in Table 2. We also conducted a qualitative evaluation. Seventeen subjects (13 males and 4 females, age 22 to 27) were recruited from a local university. We asked each subject to compare each projected result and corresponding target appearance, and rate the perceived contrast according to a 9-point Likert scale from 1 (very low contrast) to 9 (high contrast same as the target appearance). The projected result (rectified as shown in Fig. 9) and target appearance are shown on a flat panel 46-inch display (Panasonic LC-46LX3) side by side. Figure 11 shows the averages and standard deviations of the perceived contrasts of the four (i.e., complex, dog, room, and meal) images of the three (i.e., direct, projection only, and proposed) methods. A one-way analysis of variance (ANOVA) with repeated measures showed the projection method had a significant effect on the perceived contrast in all image conditions (complex: $F_{2,32} = 8.99, p < 0.01$, dog: $F_{2,32} = 5.34, p < 0.05$, room: $F_{2,32} = 17.93, p < 0.01$, meal: $F_{2,32} = 7.74, p < 0.01$). Post-hoc analysis was then performed using a Student-Newman-Keuls test for pairwise comparison. It showed statistically significant differences between the proposed method and each of the other two methods in all image conditions ($p < 0.05$). The observations described in the previous paragraph are supported by both the SSIM values and the perceived contrasts. Compared to the other two methods, the proposed method always provided the best image qualities in terms of similarity to the target images as well as contrast.

5 Discussion

Through the simulation and physical experiments, we have confirmed the potential of the proposed method to improve image quality in immersive projection display systems by reducing the artifacts caused by the inter-reflection of projected light. In the simulation experiment with an L-shaped corner screen, the proposed method achieved MSEs that were 1/24 and 1/2 that of the direct and projection only methods respectively. For cylinder and dome screens, we have confirmed that the proposed method improves the projected image qualities. However, the degree of improvement is less significant than that for the L-shaped corner screen. Therefore, the proposed method is particularly effective and useful for an immersive projection display with a screen

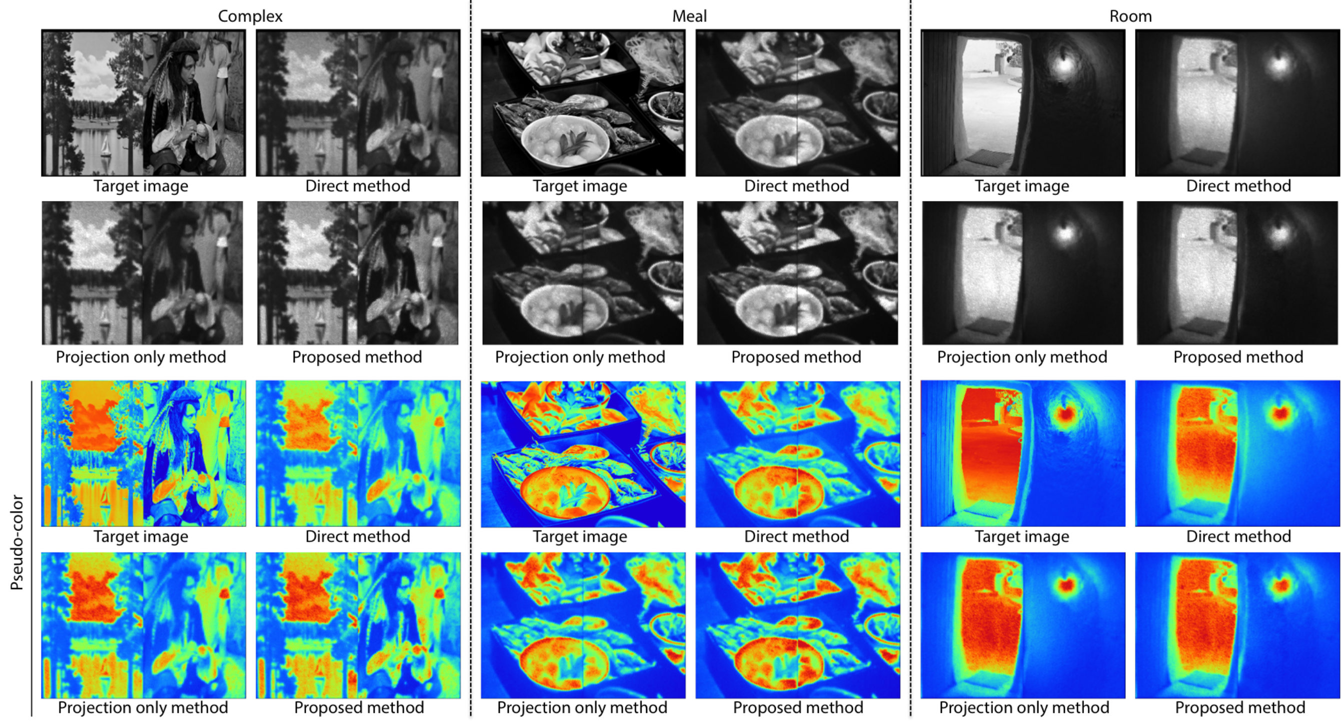

Fig. 9. Experimental results. The pseudo-color representation visualizes the intensity values of the projected results from blue (dark) to red (bright).

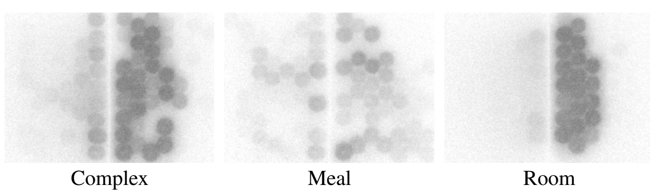

Fig. 10. Displayed reflectance pattern.

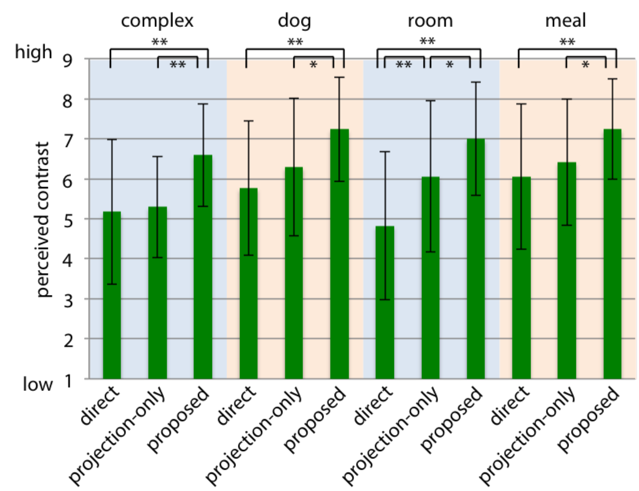

Fig. 11. Qualitative evaluation result: the average and standard deviation of perceived contrast (**: $p < 0.01$, *: $p < 0.05$).

shape that has a sharp corner, such as cubic screens. Such screens have been applied in many VR systems, including CAVE.

In the physical experiment, we demonstrated the advantage of the proposed method over conventional inter-reflection compensation techniques with our proof-of-concept prototype system. However, more thorough and professional design and assembly will enhance performance. One of the practical limitations of the current implementation is its inflexibility in the size and shape of a projection screen. For the current system, we painted the PhC manually, which is obviously impractical, especially in manufacturing large PhC-painted screens. This issue can be solved by using a professional large-format photochromic printer [29]. A UV projector [10], rather than UV LEDs, has the potential to illuminate large screens of various shapes, including non-planar surfaces, such as cylinder and dome screens.

The proposed technique is useful not only for immersive VR systems but also for spatial augmented reality (SAR) or projection mapping applications. For example, consider projecting images onto an architectural model [25], a replica of a historically important object [28], or a robot head [2] to visualize how different shapes, reflectance properties, or environment illuminations affect the appearance of such objects. Showing annotations on such objects to allow users to easily understand them is also regarded as an important application in AR [15]. Generally, such objects have a concave shape; thus, the projected results usually suffer from inter-reflections. By applying the proposed technique by painting objects with PhCs and preparing a UV projector, many of the artifacts caused by inter-reflections can be removed; consequently, we can enhance the image quality of the projected results.

When calibrating the reflectance pattern modulation component in the physical experiment, we found that the current PhC has a contrast ratio of approximately 2:1. Furthermore, the PhC used in the experiment was very slow (1 minute for modulation; see 4.2). A better PhC with higher contrast—lower reflectance—and faster response can enhance the performance of the inter-reflection compensation. Although the PhCs used in our experiment are commercially available, researchers in chemistry and molecular science are working on synthesizing high contrast (>30:1) and high speed (several milliseconds) PhCs for holographic data storage and/or real-time 3D holographic displays [1, 20]. We believe that there will be a better material whose displayable minimum reflectance is much smaller than the current technology, which will improve the inter-reflection compensation performance.

Each iteration process took about 1 second in the optimization process (see 4.1). Therefore, the proposed method works only for pre-rendered movies. The bottleneck of the process is the computation of Eq. 12, which represents the forward radiosity process. We can speed up this process by applying a real-time global illumination algorithm such as [16] to display interactive VR contents on our proposed system.

6 Conclusion

In this paper, we have proposed an inter-reflection compensation technique for immersive projection displays, in which we spatially modulate the screen reflectance pattern to improve the compensation performance of conventional methods. Through simulation and physical experiments, we have confirmed that the combination of reflectance pattern modulation and a conventional inter-reflection compensation technique can enhance the compensation performance compared to the projector compensation technique. We can display images on various concave screens with MSEs half that of a conventional method on average. We believe that this research shows a promising application field to chemistry and molecular science researchers, and we hope to stimulate further development of better PhCs to decrease the displayable minimum reflectance. In future, we plan to increase the size of the system by applying a professional PhC printer and UV projector to develop a real scale immersive projection system.

Acknowledgments

This work was supported by JSPS KAKENHI Grant Number 15H05925 (Grant-in-Aid for Scientific Research on Innovative Areas Innovative SHITSUKAN Science and Technology).

References

[1] K. Arai, Y. Kobayashi, and J. Abe. Rational molecular designs for drastic acceleration of the color-fading speed of photochromic naphthopyrans. *Chemical Communications*, 51:3057–3060, 2015.

[2] A. Bermano, P. Brüschweiler, A. Grundhöfer, D. Iwai, B. Bickel, and M. Gross. Augmenting Physical Avatars Using Projector Based Illumination. *ACM Transactions on Graphics*, 32(6):189:1–189:10, 2013.

[3] O. Bimber, A. Grundhöfer, T. Zeidler, D. Danch, and P. Kapakos. Compensating Indirect Scattering for Immersive and Semi-immersive Projection Displays. In *Proceedings of the IEEE Virtual Reality Conference (IEEE VR)*, pages 151–158, 2006.

[4] O. Bimber and D. Iwai. Superimposing Dynamic Range. *ACM Transactions on Graphics*, 27(5):150:1–150:8, 2008.

[5] O. Bimber, D. Iwai, G. Wetzstein, and A. Grundhöfer. The Visual Computing of Projector-Camera Systems. *Computer Graphics Forum*, 27(8):2219–2254, 2008.

[6] O. Bimber, D. Klöck, T. Amano, A. Grundhöfer, and D. Kurz. Closed-Loop Feedback Illumination for Optical Inverse Tone-Mapping in Light Microscopy. *IEEE Transactions on Visualization and Computer Graphics*, 17(6):857–870, 2011.

[7] C. M. Goral, K. E. Torrance, D. P. Greenberg, and B. Battaile. Modeling the interaction of light between diffuse surfaces. In *Proceedings of ACM SIGGRAPH*, pages 213–222, 1984.

[8] A. Grundhöfer and D. Iwai. Robust, error-tolerant photometric projector compensation. *IEEE Transactions on Image Processing*, 24(12):5086–5099, 2015.

[9] H. Habe, N. Saeki, and T. Matsuyama. Inter-reflection compensation for immersive projection display. In *Proceedings of the IEEE International Workshop on Projector-Camera Systems (ProCams)*, 2007.

[10] T. Hashida, Y. Kakehi, and T. Naemura. Photochromic sculpture: volumetric color-forming pixels. In *Proceedings of ACM SIGGRAPH Studio Talks*, page 11:1, 2011.

[11] R. Hoskinson, B. Stoeber, W. Heidrich, and S. Fels. Light reallocation for high contrast projection using an analog micromirror array. *ACM Transactions on Graphics*, 29(6):165:1–165:10, 2010.

[12] D. Iwai, S. Mihara, and K. Sato. Extended depth-of-field projector by fast focal sweep projection. *IEEE Transactions on Visualization and Computer Graphics*, 21(4):462–470, 2015.

[13] D. Iwai, M. Nagase, and K. Sato. Shadow removal of projected imagery by occluder shape measurement in a multiple overlapping projection system. *Virtual Reality*, 18(4):245–254, 2014.

[14] D. Iwai, S. Takeda, N. Hino, and K. Sato. Projection Screen Reflectance Control for High Contrast Display using Photochromic Compounds and UV LEDs. *Optics Express*, 22(11):13492–13506, 2014.

[15] D. Iwai, T. Yabiki, and K. Sato. View management of projected labels on non-planar and textured surfaces. *IEEE Transactions on Visualization and Computer Graphics*, 19(8):1415–1424, 2013.

[16] A. Kaplanyan and C. Dachsbacher. Cascaded light propagation volumes for real-time indirect illumination. In *Proceedings of the ACM SIGGRAPH symposium on Interactive 3D Graphics and Games (I3D)*, pages 99–107, 2010.

[17] Y. Kusakabe, M. Kanazawa, Y. Nojiri, M. Furuya, and M. Yoshimura. YC-separation Type Projector with Double Modulation. In *Proc. of International Display Workshop (IDW)*, pages 1959–1962, 2006.

[18] Y. Li, Q. Yuan, and D. Lu. Perceptual Radiometric Compensation for Inter-reflection in Immersive Projection Environment. In *Proceedings of the ACM Symposium on Virtual Reality Software and Technology (VRST)*, pages 201–208, 2013.

[19] A. Majumder and M. S. Brown. *Practical Multi-Projector Display Design*. A. K. Peters Ltd., 2007.

[20] N. Malic and R. A. Evans. The use of poly(alkylene oxide)s to achieve fast and controlled photochromic switching in rigid matrices. *Journal of Polymer Science Part A: Polymer Chemistry*, 50(7):1434–1444, 2012.

[21] S. Mihara, D. Iwai, and K. Sato. Artifact reduction in radiometric compensation of projector-camera systems for steep reflectance variations. *IEEE Transactions on Circuits and Systems for Video Technology*, 24(9):1631–1638, 2014.

[22] Y. Mukaigawa, T. Kakinuma, and Y. Ohta. Analytical Compensation of Inter-reflection for Pattern Projection. In *Proceedings of the ACM Symposium on Virtual Reality Software and Technology (VRST)*, pages 265–268, 2006.

[23] M. Nagase, D. Iwai, and K. Sato. Dynamic defocus and occlusion compensation of projected imagery by model-based optimal projector selection in multi-projection environment. *Virtual Reality*, 15(2-3):119–132, 2011.

[24] T.-T. Ng, R. S. Pahwa, J. Bai, K.-H. Tan, and R. Ramamoorthi. From the Rendering Equation to Stratified Light Transport Inversion. *International Journal of Computer Vision*, 96(2):235–251, 2012.

[25] R. Raskar, G. Welch, K.-L. Low, and D. Bandyopadhyay. Shader lamps: Animating real objects with image-based illumination. In *Proceedings of Eurographics Workshop on Rendering Techniques*, pages 89–102, 2001.

[26] H. Seetzen, W. Heidrich, W. Stuerzlinger, G. Ward, L. Whitehead, M. Trentacoste, A. Ghosh, and A. Vorozcovs. High dynamic range display systems. In *Proceedings of ACM SIGGRAPH*, pages 760–768, 2004.

[27] Y. Sheng, T. C. Yapo, and B. Cutler. Global illumination compensation for spatially augmented reality. *Computer Graphics Forum*, 29(2):387–396, 2010.

[28] S. Shimazu, D. Iwai, and K. Sato. 3D High Dynamic Range Display System. In *Proceedings of the IEEE International Symposium on Mixed and Augmented Reality (ISMAR)*, pages 235–236, 2011.

[29] SO-KEN Corporation, 2015. `http://soken-creative.com/` (in Japanese).

[30] H. A. van der Vorst. Bi-cgstab: A fast and smoothly converging variant of bi-cg for the solution of nonsymmetric linear systems. *SIAM Journal on Scientific and Statistical Computing*, 13(2):631–644, 1992.

[31] Z. Wang, A. C. Bovik, H. R. Sheikh, and E. P. Simoncelli. Perceptual image quality assessment: from error visibility to structural similarity. *IEEE Transactions on Image Processing*, 13(4):600–612, 2004.

[32] G. Wetzstein and O. Bimber. Radiometric Compensation through Inverse Light Transport. In *Proceedings of Pacific Conference on Computer Graphics and Applications*, pages 391–399, 2007.